



Original software publication

# galkin: A new compilation of Milky Way rotation curve data

Miguel Pato<sup>a,\*</sup>, Fabio Iocco<sup>b</sup><sup>a</sup> The Oskar Klein Centre for Cosmoparticle Physics, Department of Physics, Stockholm University, AlbaNova, SE-106 91 Stockholm, Sweden<sup>b</sup> ICTP South American Institute for Fundamental Research, and Instituto de Física Teórica - Universidade Estadual Paulista (UNESP), Rua Dr. Bento Teobaldo Ferraz 271, 01140-070 São Paulo, SP, Brazil

## ARTICLE INFO

## Article history:

Received 2 August 2016

Received in revised form

19 December 2016

Accepted 22 December 2016

## Keywords:

Dark matter

Galaxy: kinematics and dynamics

## ABSTRACT

We present *galkin*, a novel compilation of kinematic measurements tracing the rotation curve of our Galaxy together with a tool to treat the data. The compilation is optimised to Galactocentric radii between 3 and 20 kpc and includes the kinematics of gas, stars and masers in a total of 2780 measurements carefully collected from almost four decades of literature. A simple, user-friendly tool is provided to select, treat and retrieve the full database.

© 2016 Published by Elsevier B.V.

## Code metadata

Current code version	v1.0
Permanent link to code/repository used for this code version	<a href="https://github.com/ElsevierSoftwareX/SOFTX-D-16-00063">https://github.com/ElsevierSoftwareX/SOFTX-D-16-00063</a>
Legal Code License	GNU General Public License 3
Code versioning system used	Git
Software code languages, tools, and services used	Python
Compilation requirements, operating environments & dependencies	Python packages: matplotlib, numpy, wx (when using the graphic interface, see Section 3), astropy (if desired by the user, see Section 2.1)
If available Link to developer documentation/manual	None
Support email for questions	<a href="mailto:galkin.tool.mw@gmail.com">galkin.tool.mw@gmail.com</a>

## 1. Motivation and significance

The rotation curve of a spiral galaxy provides far-reaching insight into its properties, as noticeably explored for decades now (see e.g. Refs. [1–5]). Data on the rotation curve of the Milky Way – a spiral itself – have also been available for several decades [6–11]. However, the data are rather disperse throughout the literature and groups of references are often neglected. We therefore set out to assemble a comprehensive compilation of the decades-long observational effort to pinpoint the rotation curve of the Milky Way. The compilation improves upon existing ones (e.g. Refs. [12,13]) on several aspects, including most notably: (i) an enlarged database of observations appropriately treated for unified use, and (ii) the release of a simple out-of-the-box tool to retrieve

the data.<sup>1</sup> This compilation has been first used in Ref. [14] and later adopted in other works in the literature – see Section 4 for more on the impact of *galkin*. Without venturing into any analysis of the Galactic structure or dynamics (as done in *galpy* [15]), here we provide instead a thorough description of the data sets as well as the features of an out-of-the-box tool to access the database and output the desired data for independent analyses. The open source code provided is simple, flexible and can be easily modified to include new data sets or other types of measurements. The latter feature is particularly relevant on the eve of the precision era soon to be introduced by the Gaia satellite [16] and an array of optical and near-infrared ground-based surveys such as APOGEE-2 [17,18], GALAH [19], WEAVE [20] and 4MOST [21]. Our compilation can be regarded as a step forward in unifying the current state of the art, yet it is certainly susceptible of further

\* Corresponding author.

E-mail address: [migpato@gmail.com](mailto:migpato@gmail.com) (M. Pato).<sup>1</sup> To download your copy of *galkin*, please refer to our GitHub page [github.com/galkintool/galkin](https://github.com/galkintool/galkin) or contact us at [galkin.tool.mw@gmail.com](mailto:galkin.tool.mw@gmail.com).

**Table 1**

The list of all kinematic measurements of the Milky Way included in `galkin`. For each reference, the range of Galactocentric radius is reported assuming  $R_0 = 8$  kpc along with the Galactic quadrant(s) covered and the number of tracers selected out of the total original samples. In this context, the term “tracers” denotes observed objects or regions (i.e. terminal points, clouds, clusters, stars or masers) which allow for a measurement of the rotation curve of the Galaxy. For the sources signalled with †, in addition to the line-of-sight velocities, we also process the measured proper motions.

	Tracer type	$R$ [kpc]	Quadrants	Tracers
Gas kinematics	HI terminal velocities			
	Fich+ '89 [10]	2.1–8.0	1, 4	149/149
	Malhotra '95 [22]	2.1–7.5	1, 4	110/110
	McClure–Griffiths & Dickey '07 [23]	2.8–7.6	4	701/761
	HI thickness method			
	Honma & Sofue '97 [24]	6.8–20.2	–	13/13
	CO terminal velocities			
	Burton & Gordon '78 [7]	1.4–7.9	1	284/284
	Clemens '85 [8]	1.9–8.0	1	143/143
	Knapp+ '85 [9]	0.6–7.8	1	37/37
	Luna+ '06 [25]	2.0–8.0	4	272/457
	HII regions			
	Blitz '79 [6]	8.7–11.0	2, 3	3/3
	Fich+ '89 [10]	9.4–12.5	3	5/104
	Turbide & Moffat '93 [26]	11.8–14.7	3	5/8
	Brand & Blitz '93 [27]	5.2–16.5	1, 2, 3, 4	148/206
	Hou+ '09 [28]	3.5–15.5	1, 2, 3, 4	274/815
Giant molecular clouds				
Hou+ '09 [28]	6.0–13.7	1, 2, 3, 4	30/963	
Star kinematics	Open clusters †			
	Frinchaboy & Majewski '08 [29]	4.6–10.7	1, 2, 3, 4	60/71
	Planetary nebulae			
	Durand+ '98 [30]	3.6–12.6	1, 2, 3, 4	79/867
	Classical cepheids			
	Pont+ '94 [11]	5.1–14.4	1, 2, 3, 4	245/278
	Pont+ '97 [31]	10.2–18.5	2, 3, 4	32/48
Carbon stars				
Demers & Battinelli '07 [32]	9.3–22.2	1, 2, 3	55/103	
Battinelli+ '13 [33]	12.1–24.8	1, 2	35/36	
Masers	Masers †			
	Reid+ '14 [34]	4.0–15.6	1, 2, 3, 4	80/103
	Honma+ '12 [35]	7.7–9.9	1, 2, 3, 4	11/52
	Stepanishchev & Bobylev '11 [36]	8.3	3	1/1
	Xu+ '13 [37]	7.9	4	1/30
Bobylev & Bajkova '13 [38]	4.7–9.4	1, 2, 4	7/31	

inclusions – please see our own extensive caveats and notes throughout the manuscript. We encourage the community to adopt `galkin` and participate in its extension as new data sets arise.

## 2. Software description

The `galkin` compilation has three main categories of data: (i) *gas kinematics*, including HI terminal velocities [10,22,23], HI thickness [24], CO terminal velocities [7–9,25], HII regions [6,10,26–28], and giant molecular clouds [28]; (ii) *star kinematics*, including open clusters [29], planetary nebulae [30], classical cepheids [11,31], and carbon stars [32,33]; and (iii) *masers* [34–38]. Table 1 recaps the key features of each data set. Appendix A gives a full account of our data selection and treatment for each reference listed in Table 1.

Our compilation consists of 2780 tracers distributed in Galactocentric radius  $R$ , Galactic longitude  $\ell$  and height  $z$  above Galactic plane as shown in Fig. 1. Each object is specified by its coordinates  $(\ell, b)$ , heliocentric distance  $d$  and heliocentric line-of-sight velocity  $v_h^{\text{los}}$ . The uncertainties on  $\ell$  and  $b$  are largely subleading and hence neglected, whereas the uncertainties on  $d$  and  $v_h^{\text{los}}$  are taken from the original references (cf. details in Appendix A). In radio observations, it is customary to report measurements of  $v_h^{\text{los}}$  in terms of the line-of-sight velocity in the local standard of rest (LSR)  $v_{\text{lsr}}^{\text{los}}$  for a fixed peculiar solar motion  $(U, V, W)_{\odot}$  (where the subscript  $\odot$  denotes a solar value). In these cases, we infer  $v_h^{\text{los}}$  by subtracting the peculiar solar motion used in the reference off the reported  $v_{\text{lsr},0}^{\text{los}}$  (cf. Appendix A). Once  $v_h^{\text{los}}$  is obtained, this is

summed to the adopted peculiar solar motion to get the final LSR line-of-sight velocity  $v_{\text{lsr}}^{\text{los}}$ . Each object has an associated measurement  $(\ell, b, d \pm \Delta d, v_{\text{lsr}}^{\text{los}} \pm \Delta v_{\text{lsr}}^{\text{los}})$ . The corresponding Galactocentric radius follows from simple geometry as

$$R = (d^2 \cos^2 b + R_0^2 - 2R_0 d \cos b \cos \ell)^{1/2}, \quad (1)$$

where  $R_0$  is the distance of the Sun to the Galactic centre. Under the assumption of circular orbits, the angular circular velocity of the object  $\omega_c$  is found by inverting

$$v_{\text{lsr}}^{\text{los}} = (R_0 \omega_c - v_0) \cos b \sin \ell, \quad (2)$$

where  $v_0$  is the local circular velocity. The uncertainties on  $d$  and  $v_{\text{lsr}}^{\text{los}}$  are propagated to  $R$  and  $\omega_c$ , respectively. We shall also provide the familiar circular velocity  $v_c \equiv R\omega_c$  and corresponding uncertainties, but note that the errors of  $R$  and  $v_c$  are strongly positively correlated, while those of  $R$  and  $\omega_c$  are independent. All uncertainties currently implemented in `galkin` are symmetric following the information available in each reference; future data might provide the full distribution of observables, which would then be treated in upcoming versions of `galkin` and would be of great value for Bayesian studies. The procedure described above is common to all object types in Table 1, with some modifications in two cases. For terminal velocities, we set  $b = 0$  and  $R = R_0 |\sin \ell|$  (or, equivalently,  $d = R_0 |\cos \ell|$ ) in Eqs. (1) and (2), and each measurement reads  $(\ell, v_{\text{lsr}}^{\text{los}} \pm \Delta v_{\text{lsr}}^{\text{los}})$ . For the HI thickness method, the measured quantity is  $W \equiv R_0 \omega_c - v_0$  instead of  $v_{\text{lsr}}^{\text{los}}$ , so each data point is defined by  $(R/R_0 \pm \Delta R/R_0, W \pm \Delta W)$ , cf. Refs. [24,40]. We also process the proper motions  $\mu_{\ell^*}, \mu_b$

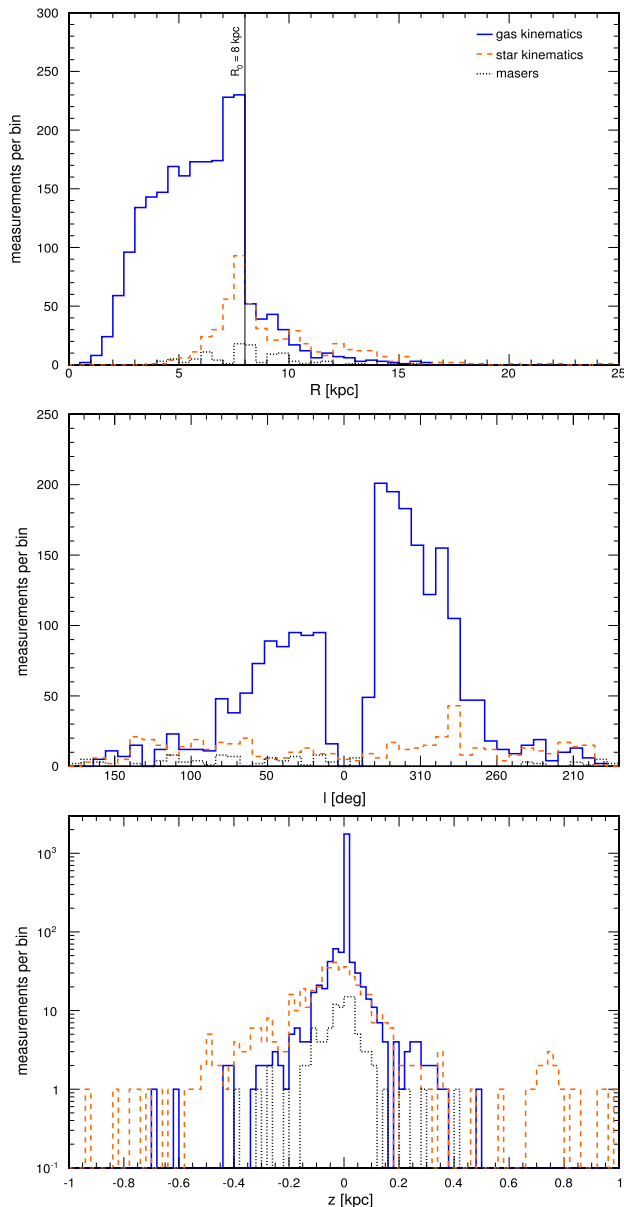


**Fig. 1.** The distribution of all kinematic tracers of the compilation in Galactocentric radius (top), Galactic longitude (centre) and height above Galactic plane (bottom). In each panel the blue solid, orange dashed and black dotted lines correspond to gas kinematics, star kinematics and masers, respectively. The leftmost distribution is obtained for  $R_0 = 8$  kpc.

when available, as is the case of open clusters and masers. All other details of data treatment are exhaustively documented in [Appendix A](#).

Note that Eqs. (1) and (2) can be used to infer  $(R, \omega_c)$  only upon fixing of  $R_0$ ,  $v_0$  and  $(U, V, W)_\odot$ , which are quantities still affected by sizeable uncertainties – see Refs. [34,41–43] for  $R_0$ , Refs. [34,44–48] for  $v_0$  and Refs. [34,39,48,49] for  $(U, V, W)_\odot$ . Making the reasonable choice of Galactic parameters  $R_0 = 8$  kpc,  $v_0 = 230$  km/s and  $(U, V, W)_\odot = (11.10, 12.24, 7.25)$  km/s [39], we show in [Fig. 2](#) the positions and circular velocities of all tracers implemented. This is the main output of *galkin*.

### 2.1. Software architecture

We now turn to the description of the *galkin* tool, whose function is to allow the user to access the data described above in a customisable way. The tool is written in Python

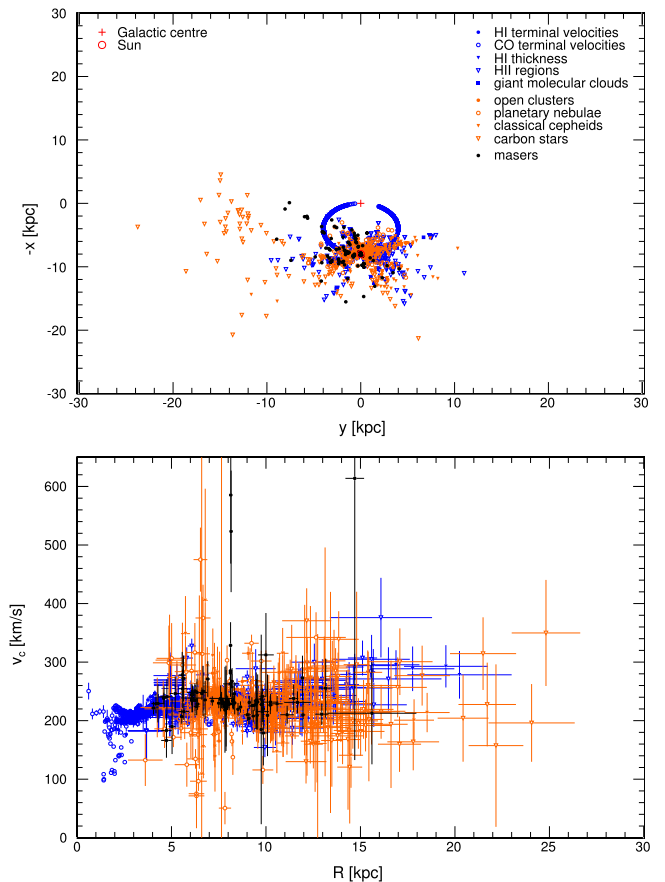


**Fig. 2.** The rotation curve of the Milky Way as derived from gas kinematics (blue), star kinematics (orange) and masers (black). The top panel shows the positions of the different tracers in the Galactic plane assuming  $R_0 = 8$  kpc. The Galactic centre sits at  $(x, y) = (0, 0)$  kpc, while the Sun position is  $(x, y) = (8, 0)$  kpc. The bottom panel displays the circular velocities of the tracers as a function of the Galactocentric radius assuming  $R_0 = 8$  kpc,  $v_0 = 230$  km/s and  $(U, V, W)_\odot = (11.10, 12.24, 7.25)$  km/s [39]. The full data displayed here is accessible via the *galkin* tool available through our GitHub page [github.com/galkintool/galkin](https://github.com/galkintool/galkin). (For interpretation of the references to colour in this figure legend, the reader is referred to the web version of this article.)

and the code package is available through our GitHub page [github.com/galkintool/galkin](https://github.com/galkintool/galkin).

The distribution has a very simple structure. The parent directory contains the setup file `setup.py` together with the usual README file. The *galkin* package is provided under `galkin/`, where `galkin/data/` contains the original data as extracted from the corresponding references,<sup>2</sup> and example scripts can be found under `bin/`. The main dependencies and installation instructions are described in the README file, whereas here we simply summarise the usage of the tool assuming it is properly installed and running. Note that *galkin* adopts *astropy* [50] for coordinate conversion if required by the user, but the code can also be used without installing this package, which is the default option.

### 2.2. Software functionalities

The goal of *galkin* is to provide ready-to-use data files containing all the necessary kinematic tracer information for

<sup>2</sup> Note that the main point of this tool is to handle in a unified way data from references using different Galactic parameters, different definitions, and which often overlap databases of observed sources. The data files under `data/` contain the original published data of each reference; please do not use these files directly unless you are fully aware of all details of each reference.

constraining the rotation curve of the Galaxy. The user may choose the values for the Galactic parameters ( $R_0$ ,  $v_0$ ) and  $(U, V, W)_\odot$ , as well as (de)select either entire classes of tracers (gas, stars, masers) or single references in Table 1. It is also possible to add a given systematic uncertainty to the line-of-sight velocity of each tracer. In summary, `galkin` has two main functionalities: to retrieve the kinematic data from the selected tracers appropriately treated for unified use, and to plot the kinematic and positional data of the selected tracers. The use of each functionality is illustrated with specific examples in the Section 3.

### 3. Illustrative examples

The user input is done with the help of the script `bin/galkin_data.py` either through a graphic interface by launching the tool from `bin/` with the command

```
python galkin_data.py
```

or through a customisable input file by typing

```
python galkin_data.py inputpars.txt
```

The code then processes the original data sets of the selected references converting each data set consistently for the chosen values of the Galactic parameters. The output is stored in three data files:

- `bin/output/posdata.dat` with the position information of each tracer, namely  $(R, d, \ell, b, x, y, z)$ ;
- `bin/output/vcdata.dat` with the rotation curve measurements, namely  $(R, \Delta R, v_c, \Delta v_c, \omega_c, \Delta \omega_c)$ ; and
- `bin/output/rawdata.dat` with the raw data measurements, namely  $(v_{\text{los}}, \Delta v_{\text{los}}, \mu_{\ell^*}, \Delta \mu_{\ell^*}, \mu_b, \Delta \mu_b)$ .

In the first two files, the values of the Galactic parameters chosen by the user are reported in the first line and the source reference for each tracer is indicated in the last column. For testing purposes, we provide under `bin/output/` the sample files corresponding to our baseline choice of Galactic parameters used to produce Fig. 2 (for the entire database and single classes objects, separately) as well as for a variation of the Galactic parameters (for the entire database only).

The tool also includes the script `bin/galkin_plotter.py` to read and visualise the output described above. This can be launched from `bin/` with the command

```
python galkin_plotter.py output/vcdata.dat output/posdata.dat
```

which produces a set of demonstrative plots including the spatial distribution of the tracers and the inferred rotation curve.

Finally, we provide the script `bin/galkin_data_fast.py` in order to illustrate how to use `galkin` inside another code without dealing with input nor output files. This is a faster version of the data processing pipeline that is specifically designed for applications that need to use `galkin` repeatedly, e.g. in scans over Galactic parameters.

### 4. Impact

The software presented here was specifically designed to study in detail the kinematics of the Milky Way. Two simple features make `galkin` particularly useful in this respect. First, the software permits a fast, self-consistent and efficient conversion of all the data sets for a unified scan of the Galactic parameters. This has notable importance today since the Galactic parameters represent one of the leading sources of uncertainty in studying the dynamics of the Galaxy [51]. Second, the thorough labelling of the different types of kinematic tracers permits their simple and automated selection, an important tool to test the (possible) bias introduced by different data sets. The compilation at the base

of `galkin` has been used to infer the dark matter content in the Galaxy and to test the robustness of existing analysis against selection effects [51–53]. Moreover, the software has already reached beyond the restricted community of originally targeted users to run extensive automated analysis, for instance improving the criterion for the selection of Milky Way analogues in some of the latest high-resolution hydrodynamical simulations [54,55]. We believe `galkin` is the first step to revisit old questions and tackle new challenges in understanding the Milky Way kinematics as the next generation of satellite-borne and ground-based astronomical surveys sets in.

The rationale behind our literature survey is to be as exhaustive as possible, but still selective enough to put together a clean and reliable sample of kinematic tracers. For that reason, we have decided to exclude objects with kinematic distance determination only, important asymmetric drift or large random motions. Whereas we have taken utter care in making such compilation exhaustive, we cannot exclude that some data sets may be missing; the reader compelled to add extra data sets is welcome to do so by modifying the open source code described in here. Our compilation is focused on the range of Galactocentric radii  $R = 3\text{--}20$  kpc and is not intended for use far outside this range. In particular, compilations dedicated to the very internal regions of the Milky Way are available elsewhere in the literature [56]. However, we warn the reader that the use of kinematic tracers at  $R \lesssim 2\text{--}5$  kpc may be problematic for certain applications [57].

Note as well that kinematic tracers beyond the ones in our compilation exist and are discussed at length in the literature, including tracers in the inner and outer halo [13,58–61], disc [48, 62–64] and off the Galactic plane [65–69]. For careful analyses of the implications of these and other tracers on the mass distribution of the Milky Way, we refer the reader to the works cited above and also to Refs. [49,70–83], where the authors have often times built their own tracer compilations. Partial compilations are easily reproducible with the `galkin` tool given the possibility to (de-)select individual references. Also, the code we provide is modular and easily modifiable for the inclusion of additional data sets in upcoming versions of `galkin` or by the user.

### 5. Conclusions

The structure of `galkin` is purposely minimal and modular. The code can be easily adapted to replace or modify existing data sets or single tracers and to add new data sets as they become available. The idea behind `galkin` is to provide a user-friendly compilation of tracers of the kinematics of the Milky Way, which will be kept up to date over the coming years.

### Acknowledgements

M.P. acknowledges the support from Wenner-Gren Stiftelsen in Stockholm; F.I. is supported by FAPESP JP project 2014/11070-2.

### Appendix A. Data treatment

Tracers of the rotation curve of the Milky Way usually adopted in the literature can be roughly divided into three categories: gas kinematics, kinematics of stellar objects, and masers. For each of these classes of objects, different methodologies are used to infer positions, distances and kinematics. Without attempting here a review of the properties of each tracer type, we point to the Supplementary Information of Ref. [14], where this collection of data has first been presented. The reader will find there an in-depth description of all tracer types as well as appropriate references to the original literature. In this Appendix, we recap the original source references and fully document our data treatment. Let us

notice that halo stars are currently not included in this version of `galkin`, due to the additional assumptions needed. Future versions of the code will properly include halo stars as an extra tracer type.

**Table 1** displays the key features of all data sets used in `galkin`. In order to obtain a clean sample, we have imposed various data selection cuts on the available sources following closely the recommendations of each original reference (notice, however, that the interested user can easily override these software cuts hacking the source code directly). The distribution of the tracers in Galactocentric radius, Galactic longitude and height above Galactic plane is shown in **Fig. 1**. In the following we provide a detailed description of the treatment applied to each data set listed in **Table 1**. Equation, figure and table numbering refers to the original source references.

## A.1. Gas kinematics

### A.1.1. HI terminal velocities

**Fich+ '89 [10]**. From **Tab. 2**, we take the terminal velocities  $v_{\text{lsr},0}^{\text{los}}$  measured at different longitudes  $\ell$  and assume an overall velocity uncertainty  $\Delta v_{\text{lsr}}^{\text{los}} = 4.5$  km/s following **Sec. II.b.i**. The reported velocities  $v_{\text{lsr},0}^{\text{los}}$  correspond to a peculiar solar motion  $(U, V, W)_{\odot} = (10.3, 15.3, 7.7)$  km/s, which is consistently subtracted off in our compilation.<sup>3</sup> We further correct for the peculiar LSR motion of 4.2 km/s in the radial direction, cf. **Sec. II.b.i** and **Eq. (4)**.<sup>4</sup>

**Malhotra '95 [22]**. From **Fig. 7**, we take the terminal velocities  $v_{\text{lsr},0}^{\text{los}}$  measured at different Galactocentric radii  $R/R_0$  and assume an overall velocity uncertainty  $\Delta v_{\text{lsr}}^{\text{los}} = 9$  km/s in line with the dispersions computed in **Sec. 3.4** for both the first and fourth quadrants. The Galactocentric radii are converted into longitudes through  $R = R_0 |\sin \ell|$  depending on the quadrant (first quadrant: circles and triangles in top panel of **Fig. 7**; fourth quadrant: squares in bottom panel of **Fig. 7**). The reported velocities  $v_{\text{lsr},0}^{\text{los}}$  correspond to a peculiar solar motion  $(U, V, W)_{\odot} = (10.3, 15.3, 7.7)$  km/s, which is consistently subtracted off in our compilation (see footnote 3).

**McClure–Griffiths & Dickey '07 [23]**. From **Tab. 1** (online version), we take the terminal velocities  $v_{\text{lsr},0}^{\text{los}}$  measured at different longitudes  $\ell$ . According to **Secs. 3.3** and **4.3.1** and the caption of **Fig. 8**, the velocity uncertainty amounts to  $\Delta v_{\text{lsr}}^{\text{los}} = 1$  km/s for  $\ell < 325^\circ$ ,  $\Delta v_{\text{lsr}}^{\text{los}} = 3$  km/s for  $\ell > 332.5^\circ$  and  $\Delta v_{\text{lsr}}^{\text{los}} = 10$  km/s for  $\ell = 327.5^\circ - 332^\circ$ ; we conservatively assume  $\Delta v_{\text{lsr}}^{\text{los}} = 10$  km/s for the whole range  $\ell = 325^\circ - 332.5^\circ$ . The reported velocities  $v_{\text{lsr},0}^{\text{los}}$  correspond to a peculiar solar motion  $(U, V, W)_{\odot} = (10.3, 15.3, 7.7)$  km/s, which is consistently subtracted off in our compilation (see footnote 3). We exclude from the full data set regions with discrete HI clouds at  $\ell = 306^\circ \pm 1^\circ$ ,  $312^\circ \pm 0.5^\circ$ ,  $320^\circ \pm 0.5^\circ$  (cf. **Sec. 4**; the width of the intervals is fixed a posteriori in order to eliminate the spikes in velocity) and also the region at  $|\sin \ell| > 0.95$  because there  $\Delta v_{\text{lsr}}^{\text{los}}/v_{\text{lsr},0}^{\text{los}} \sim 1$  (cf. **Sec. 4.2**; this last cut is actually already performed in the online version of **Tab. 1**).

<sup>3</sup> Notice that the original reference fails to indicate explicitly the adopted peculiar solar motion. Following **Ref. [45]**, we assume the adopted value is the old standard solar motion as defined in the **Appendix** of **Ref. [45]**.

<sup>4</sup> Notice that this correction depends on the assumed peculiar solar motion, so this procedure is strictly valid only when the user selects the same peculiar solar motion as in the original reference; in practice, however, this is a small correction and we ignore the slight inconsistency.

### A.1.2. HI thickness method

**Honma & Sofue '97 [24]**. From **Tab. 1**, we take the Galactocentric radii  $R/R_0$  fitted through the thickness method for different velocities  $W \equiv R_0 \omega_c - v_0$  and assume an overall uncertainty  $\Delta W = 5.8$  km/s following **Sec. 2.4**. The authors of this reference find that the method of **Merrifield '92 [40]** (i.e. method 1 in **Tab. 1**) covers the largest range of  $R/R_0$  and is the most accurate, so we use the results of that method for our compilation.

### A.1.3. CO terminal velocities

**Burton & Gordon '78 [7]**. From **Fig. 2**, we take the terminal velocities  $v_{\text{lsr},0}^{\text{los}}$  measured at different longitudes  $\ell$ , where  $v_{\text{lsr},0}^{\text{los}}$  already includes the line width correction, cf. **Sec. 3** and **Eq. (4a)**. The resolution of the original CO data presented in this reference is  $\Delta v_{\text{lsr}}^{\text{los}} = 1.3$  km/s, while it amounts to  $\Delta v_{\text{lsr}}^{\text{los}} = 2.6$  km/s for the other data sets **[84,85]** plotted in **Fig. 2** (cf. **Sec. 2**); therefore, we conservatively assume  $\Delta v_{\text{lsr}}^{\text{los}} = 2.6$  km/s all along. The reported velocities  $v_{\text{lsr},0}^{\text{los}}$  correspond to a peculiar solar motion  $(U, V, W)_{\odot} = (10.3, 15.3, 7.7)$  km/s, which is consistently subtracted off in our compilation.

**Clemens '85 [8]**. From **Tab. 2**, we take the terminal velocities  $\tilde{v}_{\text{lsr},0}^{\text{los}}$  measured at different longitudes  $\ell$  and the corresponding uncertainties  $\Delta \tilde{v}_{\text{lsr}}^{\text{los}}$ , which actually represent 0.67 of the standard deviation, cf. footnote c in **Tab. 2**. The terminal velocities  $\tilde{v}_{\text{lsr},0}^{\text{los}}$  in **Tab. 2** are uncorrected for the line width, so the true terminal velocities read  $v_{\text{lsr},0}^{\text{los}} = \tilde{v}_{\text{lsr},0}^{\text{los}} - 3$  km/s (cf. **Sec. II.c**) and the corresponding uncertainties are  $\Delta v_{\text{lsr}}^{\text{los}} = ((\Delta \tilde{v}_{\text{lsr}}^{\text{los}}/0.67)^2 + (0.6 \text{ km/s})^2)^{1/2}$ , where 0.6 km/s is the typical error in the line width correction, cf. **Sec. II.c**. The reported velocities  $v_{\text{lsr},0}^{\text{los}}$  correspond to a peculiar solar motion  $(U, V, W)_{\odot} = (10.3, 15.3, 7.7)$  km/s, which is consistently subtracted off in our compilation (see footnote 3). We further correct for the peculiar LSR motion of 7 km/s in the azimuthal direction, cf. **Sec. II.d** (see footnote 4).

**Knapp+ '85 [9]**. From **Fig. 5**, we take the terminal velocities  $v_{\text{lsr},0}^{\text{los}} \pm \Delta \tilde{v}_{\text{lsr}}^{\text{los}}$  (top panel) and the velocity dispersions  $\sigma$  (central panel) measured at different Galactocentric radii  $R/R_0$ . The statistical uncertainty of the terminal velocities is summed in quadrature to the dispersion, i.e.  $\Delta v_{\text{lsr}}^{\text{los}} = ((\Delta \tilde{v}_{\text{lsr}}^{\text{los}})^2 + \sigma^2)^{1/2}$ . The Galactocentric radii are converted into longitudes through  $R = R_0 |\sin \ell|$  considering that the data refers to the first quadrant only. The reported velocities  $v_{\text{lsr},0}^{\text{los}}$  correspond to a peculiar solar motion  $(U, V, W)_{\odot} = (10.3, 15.3, 7.7)$  km/s, which is consistently subtracted off in our compilation (see footnote 3).

**Luna+ '06 [25]**. From **Fig. 1** (top panel), we take the terminal velocities  $v_{\text{lsr},0}^{\text{los}}$  measured at different longitudes  $\ell$  and assume an overall velocity uncertainty  $\Delta v_{\text{lsr}}^{\text{los}} = 3$  km/s following **Sec. 3.1**. The reported velocities  $v_{\text{lsr},0}^{\text{los}}$  correspond to a peculiar solar motion  $(U, V, W)_{\odot} = (14.8/20.) \times (10.3, 15.3, 7.7)$  km/s, which is consistently subtracted off in our compilation (see footnote 3). We exclude from the full data set the region at  $\ell = 280^\circ - 312^\circ$  due to the influence of the Carina arm and Centaurus, cf. **Sec. III.a.iii** in **Ref. [86]**.

### A.1.4. HII regions

**Blitz '79 [6]**. From **Tab. 2**, we take the distances  $d \pm \Delta d$  and line-of-sight velocities  $v_{\text{lsr},0}^{\text{los}} \pm \Delta v_{\text{lsr}}^{\text{los}}$  corresponding to objects towards different Galactic coordinates  $(\ell, b)$ . The reported velocities  $v_{\text{lsr},0}^{\text{los}}$  correspond to a peculiar solar motion  $(U, V, W)_{\odot} = (10.3, 15.3, 7.7)$  km/s, which is consistently subtracted off in our compilation (see footnote 3). We exclude from the full data set all objects in (or coincident to objects in) **Fich+ '89**, **Turbide & Moffat '93**, **Brand & Blitz '93** and **Hou+ '09**; only three objects remain: **S148**, **S306** and **Mon R2**.

**Fich+ '89 [10].** From Tab. 1, we take the distances  $d \pm \Delta d$  and line-of-sight velocities  $v_{\text{lsr},0}^{\text{los}} \pm \Delta \tilde{v}_{\text{lsr}}^{\text{los}}$  corresponding to objects towards different Galactic coordinates  $(\ell, b)$  and add a random motion of 6.4 km/s in quadrature to  $\Delta \tilde{v}_{\text{lsr}}^{\text{los}}$  following Sec. II.i.b. The reported velocities  $v_{\text{lsr},0}^{\text{los}}$  correspond to a peculiar solar motion  $(U, V, W)_{\odot} = (10.3, 15.3, 7.7)$  km/s, which is consistently subtracted off in our compilation (see footnote 3). We further correct for the peculiar LSR motion of 4.2 km/s in the radial direction, cf. Sec. II.b.i and Eq. (4) (see footnote 4). We exclude from the full data set all objects in (or coincident to objects in) Turbide & Moffat '93 and Brand & Blitz '93.

**Turbide & Moffat '93 [26].** From Tab. 5 (for  $Z = Z(R)$ ), we take the distances  $d \pm \Delta d$  and line-of-sight velocities  $v_{\text{lsr},0}^{\text{los}} \pm \Delta v_{\text{lsr}}^{\text{los}}$  corresponding to objects towards different Galactic coordinates  $(\ell, b)$ . Note that the reported velocities  $v_{\text{lsr},0}^{\text{los}}$  correspond to Eq. (11) with  $V_{\text{mol}} = 0$  km/s and a peculiar solar motion  $(U, V, W)_{\odot} = (9, 11, 6)$  km/s, which is consistently subtracted off in our compilation. For the objects in Tab. 5 based on Refs. [1,3] therein, we further correct for the peculiar LSR motion of 4.2 km/s in the radial direction, cf. Sec. 4 and Eq. (11). We exclude from the full data set all objects in (or coincident to objects in) Brand & Blitz '93.

**Brand & Blitz '93 [27].** From Tab. 1, we take the distances  $d \pm \Delta d$  and line-of-sight velocities  $v_{\text{lsr},0}^{\text{los}} \pm \Delta \tilde{v}_{\text{lsr}}^{\text{los}}$  corresponding to objects towards different Galactic coordinates  $(\ell, b)$  and add a random motion of 6.4 km/s in quadrature to  $\Delta \tilde{v}_{\text{lsr}}^{\text{los}}$  following Sec. 3.1. The reported velocities  $v_{\text{lsr},0}^{\text{los}}$  correspond to a peculiar solar motion  $(U, V, W)_{\odot} = (10.3, 15.3, 7.7)$  km/s, which is consistently subtracted off in our compilation (see footnote 3). We exclude from the full data set objects near to the Galactic centre  $\ell = 345^{\circ} - 15^{\circ}$  or anti Galactic centre  $\ell = 165^{\circ} - 195^{\circ}$  (cf. Sec. 3.3) and nearby objects at  $d < 1$  kpc (cf. Sec. 3.3).

**Hou+ '09 [28].** From Tab. A1, we take the distances  $d \pm \Delta d$  and line-of-sight velocities  $v_{\text{lsr},0}^{\text{los}}$  corresponding to objects towards different Galactic coordinates  $(\ell, b)$  and assume an overall velocity uncertainty  $\Delta v_{\text{lsr}}^{\text{los}} = 3$  km/s. The reported velocities  $v_{\text{lsr},0}^{\text{los}}$  correspond to a peculiar solar motion  $(U, V, W)_{\odot} = (10.3, 15.3, 7.7)$  km/s, which is consistently subtracted off in our compilation (see footnote 3). We exclude from the full data set objects without stellar distances nor at the tangent points, near to the Galactic centre  $\ell = 345^{\circ} - 15^{\circ}$  or anti Galactic centre  $\ell = 165^{\circ} - 195^{\circ}$  and objects in (or coincident to objects in) Brand & Blitz '93.

#### A.1.5. Giant molecular clouds

**Hou+ '09 [28].** From Tab. A2, we take the distances  $d$  and line-of-sight velocities  $v_{\text{lsr},0}^{\text{los}}$  corresponding to objects towards different Galactic coordinates  $(\ell, b)$  and adopt an overall velocity uncertainty  $\Delta v_{\text{lsr}}^{\text{los}} = 3$  km/s and an overall relative distance uncertainty  $\Delta d/d = 20\%$ . The reported velocities  $v_{\text{lsr},0}^{\text{los}}$  correspond to a peculiar solar motion  $(U, V, W)_{\odot} = (10.3, 15.3, 7.7)$  km/s, which is consistently subtracted off in our compilation (see footnote 3). We exclude from the full data set objects without stellar distances and near to the Galactic centre  $\ell = 345^{\circ} - 15^{\circ}$  or anti Galactic centre  $\ell = 165^{\circ} - 195^{\circ}$ .

### A.2. Star kinematics

#### A.2.1. Open clusters

**Frinchaboy & Majewski '08 [29].** From Tab. 1, we take the distances  $d$  corresponding to objects towards different equatorial coordinates  $(\alpha, \delta)$  (then converted to Galactic coordinates  $(\ell, b)$ ) based on Ref. [87] and assume an overall relative distance uncertainty  $\Delta d/d = 20\%$ . From Tab. 12, we take the heliocentric

line-of-sight velocities  $v_{\text{h}}^{\text{los}} \pm \Delta v_{\text{h}}^{\text{los}}$ , where whenever possible we use the bulk kinematics derived with the three-dimensional and radial velocity membership criterion (3D+RV), and also the proper motions  $\mu_{\ell^*} \pm \Delta \mu_{\ell^*}, \mu_b \pm \Delta \mu_b$ . We exclude from the full data set objects near to the anti Galactic centre  $\ell = 160^{\circ} - 200^{\circ}$ ; NGC 1513, NGC 7654 (only one member identified, cf. Sec. 6.1); Collinder 258, Lynga 1, NGC 6250 (probably wrong memberships, cf. Sec. 6.2.3); and NGC 6416 (high residual velocity).

#### A.2.2. Planetary nebulae

**Durand+ '98 [30].** From Tab. 2 (online version), we take the heliocentric line-of-sight velocities  $v_{\text{h}}^{\text{los}} \pm \Delta v_{\text{h}}^{\text{los}}$  corresponding to objects towards different equatorial coordinates  $(\alpha, \delta)$  (then converted to Galactic coordinates  $(\ell, b)$ ). The distances  $d$  are found by cross-matching Tab. 2 to Tabs. 1 and 3 of Ref. [88], which report individually determined and statistical distances, respectively. When available, we prefer the individually determined distances (i.e. Tab. 1 of Ref. [88]), based on the methods presented in Ref. [89] with a relative uncertainty ranging from 15% to 40% (cf. Sec. 3.3 in Ref. [89]) so an overall relative distance uncertainty  $\Delta d/d = 25\%$  is adopted; when not possible, we use the statistical distance scale (i.e. Tab. 3 of Ref. [88]), for which the relative uncertainty is  $\Delta d/d = 30\%$  (cf. Sec. 5.2 in Ref. [88]). We further correct for the  $K$ -term of 5.1 km/s (cf. Eq. (4) and Tab. 3) and model the asymmetric drift with respect to the peculiar solar motion in use (i.e.  $U_{\text{ad}} = 16.0$  km/s  $- U_{\odot}$  in the radial direction and  $V_{\text{ad}} = 24.8$  km/s  $- V_{\odot}$  in the azimuthal direction; cf. Eq. (4) and Tab. 3). The error of  $K$ ,  $U_{\text{ad}}$  and  $V_{\text{ad}}$  (cf. Tab. 3) are propagated to the line-of-sight velocity  $v_{\text{h}}^{\text{los}}$ . We exclude from the full data set objects near to the Galactic centre  $\ell = 353^{\circ} - 7^{\circ}$  and off the Galactic plane  $z \geq 200$  pc (cf. Sec. 4.2); NGC 6565, M2-29, M1-46, Sa 1-8, NGC 6741, NGC 7293, Vy 2-2, NGC 6702, NGC 7094, NGC 2392, NGC 4071, NGC 6026, NGC 6302, M2-7, Th 3-14 (deficient statistical distances, cf. Sec. 5.2 in Ref. [88]; notice typo in this reference where NGC 6320 is mentioned instead of NGC 6302); BoBn 1 (atypical motion; cf. Sec. 4.1) and NGC 6567, A 8, Pu 1, M1-5 (high residual velocity).

#### A.2.3. Classical cepheids

**Pont+ '94 [11].** From Tab. 3, we take the distance moduli  $\mu$  (FW) and heliocentric line-of-sight velocities  $v_{\text{h}}^{\text{los}}$  corresponding to objects towards different Galactic coordinates  $(\ell, b)$  and assume an overall distance modulus uncertainty  $\Delta \mu = 0.23$  mag following Sec. 11.3. The distance moduli are converted to distances through  $d/\text{pc} = 10^{\mu/5+1}$ . The velocity uncertainty reads  $\Delta v_{\text{h}}^{\text{los}} = (\sigma_1^2 + \sigma_2^2)^{1/2}$ , where  $\sigma_1 = 1, 2.5, 5$  km/s depending on the method used to calculate the radial velocity (cf. Sec. 11.3) and  $\sigma_2 \sim 11.1$  km/s is the contribution of the velocity ellipsoid (cf. Sec. 11.3). We further correct for the  $K$ -term of  $-1.81$  km/s, cf. Sec. 11.6. We use the reduced sample of 266 stars (cf. Sec. 11.4 and Tab. 4) excluding objects near to the anti Galactic centre  $\ell = 160^{\circ} - 200^{\circ}$  and two further objects due to high residual velocity.

**Pont+ '97 [31].** From Tab. 1, we take the heliocentric line-of-sight velocities  $v_{\text{h}}^{\text{los}}$ , period  $P$  and colours  $V$  and  $B - V$  corresponding to objects towards different Galactic coordinates  $(\ell, b)$ . The distance moduli are found with the period-luminosity-colour relation described in Ref. [11] (FW) and the zero point given in Sec. 3.1; an overall distance modulus uncertainty  $\Delta \mu = 0.21$  mag is assumed following Sec. 3.3. The distance moduli are converted to distances through  $d/\text{pc} = 10^{\mu/5+1}$ . The velocity uncertainty reads  $\Delta v_{\text{h}}^{\text{los}} = (\sigma_1^2 + \sigma_2^2)^{1/2}$ , where  $\sigma_1 = 1(2.5)$  km/s for  $\geq 10 (<10)$  velocity measurements (cf. Tab. 1) and  $\sigma_2 \sim 11.1$  km/s is the contribution of the velocity ellipsoid (cf. Sec. 11.3 of Ref. [11]). We further add a 6 km/s systematic uncertainty (cf. Sec. 6; see also Sec. 5.3) to the derived circular velocity. We exclude from the full data set objects

near to the anti Galactic centre  $\ell = 160^\circ - 200^\circ$  and with no measured radial velocity or no  $B - V$ .

#### A.2.4. Carbon stars

**Demers & Battinelli '07 [32].** From Tab. 4 (online version), we take the heliocentric line-of-sight velocities  $v_h^{\text{los}} \pm \Delta\tilde{v}_h^{\text{los}}$  corresponding to objects towards different Galactic coordinates  $(\ell, b)$  and add a random motion of 20 km/s in quadrature to  $\Delta\tilde{v}_h^{\text{los}}$  following Sec. 5.1. From Tab. 1 (online version), we take the distances  $d$  and assume an overall relative distance uncertainty  $\Delta d/d = 10\%$  following Sec. 5.1. We exclude from the full data set objects near to the anti Galactic centre  $\ell = 170^\circ - 190^\circ$ ; stars no. 20 and 23 (nearly fast stars; cf. Sec. 5.2) and stars no. 17, 18, 27, 28, 35, 42, 52, 56, 58 and 60 (possibly belonging to Canis Major; cf. Sec. 5.2).

**Battinelli+ '13 [33].** From Tab. 1, we take the Galactocentric radii  $\tilde{R}$  (computed with  $R_0 = 7.62$  kpc) and heliocentric line-of-sight velocities  $v_h^{\text{los}} \pm \Delta\tilde{v}_h^{\text{los}}$  corresponding to objects towards different Galactic coordinates  $(\ell, b)$  and add a random motion of 20 km/s in quadrature to  $\Delta\tilde{v}_h^{\text{los}}$  following Sec. 5.1 of Ref. [32]. The Galactocentric radii  $\tilde{R}$  are converted to heliocentric distances  $d$  by inverting Eq. (1) using  $R_0 = 7.62$  kpc. We exclude from the full data set star no. 712 (probably belongs to the Sagittarius dwarf galaxy; cf. Sec. 4).

#### A.3. Masers

**Reid+ '14 [34].** From Tab. 1, we take the parallaxes  $\pi \pm \Delta\pi$ , line-of-sight velocities  $v_{\text{lsr},0}^{\text{los}} \pm \Delta\tilde{v}_{\text{lsr}}^{\text{los}}$  and equatorial proper motions  $\mu_{\alpha^*} \pm \Delta\mu_{\alpha^*}, \mu_{\delta} \pm \Delta\mu_{\delta}$  corresponding to objects towards different equatorial coordinates  $(\alpha, \delta)$  (then converted to Galactic coordinates  $(\ell, b)$ ) and add a virial motion of 7 km/s in quadrature to  $\Delta\tilde{v}_{\text{lsr}}^{\text{los}}$  following Sec. 3 in Ref. [45]. The parallaxes are converted to distances through  $d/\text{kpc} = \text{mas}/\pi$ , while the equatorial proper motions are converted to Galactic proper motions  $\mu_{\ell^*} \pm \Delta\mu_{\ell^*}, \mu_b \pm \Delta\mu_b$ . The reported velocities  $v_{\text{lsr},0}^{\text{los}}$  correspond to a peculiar solar motion  $(U, V, W)_\odot = (10.3, 15.3, 7.7)$  km/s, which is consistently subtracted off in our compilation. We further corrected for the mean peculiar motion of the masers, i.e.  $\bar{U}_s = 2.9$  km/s (cf. Tab. 4, A5) and  $\bar{V}_s = V_\odot - 17.1$  km/s (cf. Sec. 4.4). We exclude from the full data set eight masers with  $R < 4$  kpc (cf. footnote 3) and 15 outlier masers (cf. footnote 4).

**Honma+ '12 [35].** From Tab. 1, we take the parallaxes  $\pi \pm \Delta\pi$ , line-of-sight velocities  $v_{\text{lsr},0}^{\text{los}} \pm \Delta\tilde{v}_{\text{lsr}}^{\text{los}}$  and equatorial proper motions  $\mu_{\alpha^*} \pm \Delta\mu_{\alpha^*}, \mu_{\delta} \pm \Delta\mu_{\delta}$  corresponding to objects towards different Galactic coordinates  $(\ell, b)$  and add a virial motion of 7 km/s in quadrature to  $\Delta\tilde{v}_{\text{lsr}}^{\text{los}}$  following Sec. 3 in Ref. [45]. The parallaxes are converted to distances through  $d/\text{kpc} = \text{mas}/\pi$ , while the equatorial proper motions are converted to Galactic proper motions  $\mu_{\ell^*} \pm \Delta\mu_{\ell^*}, \mu_b \pm \Delta\mu_b$ . The reported velocities  $v_{\text{lsr},0}^{\text{los}}$  correspond to a peculiar solar motion  $(U, V, W)_\odot = (10.3, 15.3, 7.7)$  km/s, which is consistently subtracted off in our compilation (see footnote 3). We further corrected for the mean peculiar motion of the masers, i.e.  $\bar{U}_s = 2.9$  km/s (cf. Tab. 4, A5 in Ref. [34]) and  $\bar{V}_s = V_\odot - 17.1$  km/s (cf. Sec. 4.4 in Ref. [34]). We exclude from the full data set all objects in (or coincident to objects in) Reid+ '14.

**Stepanishchev & Bobylev '11 [36].** From Tab. 1, we take the parallaxes  $\pi \pm \Delta\pi$ , heliocentric line-of-sight velocities  $v_h^{\text{los}} \pm \Delta\tilde{v}_h^{\text{los}}$  and equatorial proper motions  $\mu_{\alpha^*} \pm \Delta\mu_{\alpha^*}, \mu_{\delta} \pm \Delta\mu_{\delta}$  corresponding to objects towards different equatorial coordinates  $(\alpha, \delta)$  (then converted to Galactic coordinates  $(\ell, b)$ ) and add a virial motion of 7 km/s in quadrature to  $\Delta\tilde{v}_h^{\text{los}}$  following Sec. 3 in Ref. [45]. The parallaxes are converted to distances through  $d/\text{kpc} = \text{mas}/\pi$ , while

the equatorial proper motions are converted to Galactic proper motions  $\mu_{\ell^*} \pm \Delta\mu_{\ell^*}, \mu_b \pm \Delta\mu_b$ . We further corrected for the mean peculiar motion of the masers, i.e.  $\bar{U}_s = 2.9$  km/s (cf. Tab. 4, A5 in Ref. [34]) and  $\bar{V}_s = V_\odot - 17.1$  km/s (cf. Sec. 4.4 in Ref. [34]). We exclude from the full data set all objects in (or coincident to objects in) Reid+ '14; only one object remains: Ori GMRA.

**Xu+ '13 [37].** From Tab. 4, we take the parallaxes  $\pi \pm \Delta\pi$ , line-of-sight velocities  $v_{\text{lsr},0}^{\text{los}} \pm \Delta\tilde{v}_{\text{lsr}}^{\text{los}}$  and equatorial proper motions  $\mu_{\alpha^*} \pm \Delta\mu_{\alpha^*}, \mu_{\delta} \pm \Delta\mu_{\delta}$  corresponding to objects towards different Galactic coordinates  $(\ell, b)$  and add a virial motion of 7 km/s in quadrature to  $\Delta\tilde{v}_{\text{lsr}}^{\text{los}}$  following Sec. 3 in Ref. [45]. The parallaxes are converted to distances through  $d/\text{kpc} = \text{mas}/\pi$ , while the equatorial proper motions are converted to Galactic proper motions  $\mu_{\ell^*} \pm \Delta\mu_{\ell^*}, \mu_b \pm \Delta\mu_b$ . The reported velocities  $v_{\text{lsr},0}^{\text{los}}$  correspond to a peculiar solar motion  $(U, V, W)_\odot = (10.3, 15.3, 7.7)$  km/s, which is consistently subtracted off in our compilation (see footnote 3). We further corrected for the mean peculiar motion of the masers, i.e.  $\bar{U}_s = 2.9$  km/s (cf. Tab. 4, A5 in Ref. [34]) and  $\bar{V}_s = V_\odot - 17.1$  km/s (cf. Sec. 4.4 in Ref. [34]). We exclude from the full data set all objects in (or coincident to objects in) Reid+ '14 and Honma+ '12; only one maser remains: DoAr21/Ophiuchus.

**Bobylev & Bajkova '13 [38].** From Tab. 1, we take the parallaxes  $\pi \pm \Delta\pi$ , line-of-sight velocities  $v_{\text{lsr},0}^{\text{los}} \pm \Delta\tilde{v}_{\text{lsr}}^{\text{los}}$  and equatorial proper motions  $\mu_{\alpha^*} \pm \Delta\mu_{\alpha^*}, \mu_{\delta} \pm \Delta\mu_{\delta}$  corresponding to objects towards different equatorial coordinates  $(\alpha, \delta)$  (then converted to Galactic coordinates  $(\ell, b)$ ) and add a virial motion of 7 km/s in quadrature to  $\Delta\tilde{v}_{\text{lsr}}^{\text{los}}$  following Sec. 3 in Ref. [45]. The parallaxes are converted to distances through  $d/\text{kpc} = \text{mas}/\pi$ , while the equatorial proper motions are converted to Galactic proper motions  $\mu_{\ell^*} \pm \Delta\mu_{\ell^*}, \mu_b \pm \Delta\mu_b$ . The reported velocities  $v_{\text{lsr},0}^{\text{los}}$  correspond to a peculiar solar motion  $(U, V, W)_\odot = (10.3, 15.3, 7.7)$  km/s, which is consistently subtracted off in our compilation (see footnote 3). We further corrected for the mean peculiar motion of the masers, i.e.  $\bar{U}_s = 2.9$  km/s (cf. Tab. 4, A5 in Ref. [34]) and  $\bar{V}_s = V_\odot - 17.1$  km/s (cf. Sec. 4.4 in Ref. [34]). We exclude from the full data set all objects in (or coincident to objects in) Reid+ '14, Honma+ '12, Stepanishchev & Bobylev '11 and Xu+ '13.

## References

- [1] Freeman KC. On the disks of spiral and so galaxies. *Astrophys J* 1970;160:811. <http://dx.doi.org/10.1086/150474>.
- [2] Roberts MS, Rots AH. Comparison of rotation curves of different galaxy types. *Astron Astrophys* 1973;26:483–5. <http://adsabs.harvard.edu/abs/1973A%26A....26..483R>.
- [3] Bosma A. The distribution and kinematics of neutral hydrogen in spiral galaxies of various morphological types [Ph.D. thesis]. Groningen Univ.; 1978. <http://adsabs.harvard.edu/abs/1978PhD.....195B>.
- [4] Rubin VC, Thonnard N, Ford Jr WK. Extended rotation curves of high-luminosity spiral galaxies. IV - systematic dynamical properties, SA through SC. *Astrophys J* 1978;225:L107–11. <http://dx.doi.org/10.1086/182804>.
- [5] Persic M, Salucci P. Rotation curves of 967 spiral galaxies. *Astrophys J Suppl* 1995;99:501. <http://dx.doi.org/10.1086/192195>, arXiv:astro-ph/9502091.
- [6] Blitz L. The rotation curve of the Galaxy to  $R = 16$  kiloparsecs. *Astrophys J* 1979;231:L115–9. <http://dx.doi.org/10.1086/183016>.
- [7] Burton WB, Gordon MA. Carbon monoxide in the galaxy. III - The overall nature of its distribution in the equatorial plane. *Astron Astrophys* 1978;63:7–27. <http://adsabs.harvard.edu/abs/1978A%26A....63....7B>.
- [8] Clemens DP. Massachusetts-stony brook Galactic plane CO survey - the Galactic disk rotation curve. *Astrophys J* 1985;295:422–8. <http://dx.doi.org/10.1086/163386>.
- [9] Knapp GR, Stark AA, Wilson RW. The global properties of the Galaxy. III - Maps of the (C-12)(O) emission in the first quadrant of the Galaxy. *Astron J* 1985;90:254–300. <http://dx.doi.org/10.1086/113729>.
- [10] Fich M, Blitz L, Stark AA. The rotation curve of the Milky Way to 2 R(0). *Astrophys J* 1989;342:272–84. <http://dx.doi.org/10.1086/167591>.
- [11] Pont F, Mayor M, Burki G. New radial velocities for classical cepheids. Local Galactic rotation revisited. *Astron Astrophys* 1994;285:415–39. <http://adsabs.harvard.edu/abs/1994A%26A....285..415P>.

- [12] Sofue Y, Honma M, Omodaka T. Unified rotation curve of the galaxy – Decomposition into de Vaucouleurs bulge, disk, dark halo, and the 9-kpc rotation dip. *Publ Astron Soc Japan* 2009;61:227. <http://dx.doi.org/10.1093/pasj/61.2.227>, arXiv:0811.0859.
- [13] Bhattacharjee P, Chaudhury S, Kundu S. Rotation curve of the Milky Way out to  $\sim 200$  kpc. *Astrophys J* 2014;785:63. <http://dx.doi.org/10.1088/0004-637X/785/1/63>, arXiv:1310.2659.
- [14] Iocco F, Pato M, Bertone G. Evidence for dark matter in the inner Milky way. *Nature Phys* 2015;11:245–8. <http://dx.doi.org/10.1038/nphys3237>, arXiv:1502.03821.
- [15] Bovy J. galpy: A python library for Galactic dynamics. *Astrophys J Suppl* 2015; 216:29. <http://dx.doi.org/10.1088/0067-0049/216/2/29>, arXiv:1412.3451.
- [16] de Bruijne JHJ. Science performance of Gaia, ESA's space-astrometry mission. *Astrophys Space Sci* 2012;341:31–41. <http://dx.doi.org/10.1007/s10509-012-1019-4>, arXiv:1201.3238.
- [17] <http://www.sdss.org/surveys/apogee-2/>.
- [18] Majewski SR, Schiavon RP, Frinchaboy PM, Allende Prieto C, Barkhouser R, Bizyaev D, et al. 2015. The apache point observatory Galactic evolution experiment, APOGEE. ArXiv e-prints, arXiv:1509.05420.
- [19] De Silva GM, Freeman KC, Bland-Hawthorn J, Martell S, de Boer EW, Asplund M, et al. The GALAH survey: scientific motivation. *Mon Not R Astron Soc* 2015; 449:2604–17. <http://dx.doi.org/10.1093/mnras/stv327>, arXiv:1502.04767.
- [20] <http://www.ing.iac.es/weave/index.html>.
- [21] de Jong RS, Bellido-Tirado O, Chiappini C, Depagne É, Haynes R, Johl D, et al. 4MOST: 4-metre multi-object spectroscopic telescope. In: Society of Photo-Optical Instrumentation Engineers (SPIE) Conference Series, vol. 8446. 2012, p. 0. <http://dx.doi.org/10.1117/12.926239>, arXiv:1206.6885.
- [22] Malhotra S. The vertical distribution and kinematics of H I and mass models of the Galactic disk. *Astrophys J* 1995;448:138. <http://dx.doi.org/10.1086/175946>, arXiv:astro-ph/9411088.
- [23] McClure-Griffiths NM, Dickey JM. Milky way kinematics. I. Measurements at the subcentral point of the fourth quadrant. *Astrophys J* 2007;671:427–38. <http://dx.doi.org/10.1086/522297>, arXiv:0708.0870.
- [24] Honma M, Sofue Y. Rotation curve of the galaxy. *Publ Astron Soc Japan* 1997; 49:453–60. <http://dx.doi.org/10.1093/pasj/49.4.453>.
- [25] Luna A, Bronfman L, Carrasco L, May J. Molecular gas, kinematics, and OB star formation in the spiral arms of the southern Milky Way. *Astrophys J* 2006;641: 938–48. <http://dx.doi.org/10.1086/500163>, arXiv:astro-ph/0512046.
- [26] Turbide L, Moffat AFJ. Precision photometry of young stellar groups towards the outer Galactic disk and the Galactic rotation curve. *Astron J* 1993;105: 1831–54. <http://dx.doi.org/10.1086/116558>.
- [27] Brand J, Blitz L. The velocity field of the outer galaxy. *Astron Astrophys* 1993; 275:67. <http://adsabs.harvard.edu/abs/1993A%26A...275...67B>.
- [28] Hou LG, Han JL, Shi WB. The spiral structure of our Milky Way galaxy. *Astron Astrophys* 2009;499:473–82. <http://dx.doi.org/10.1051/0004-6361/200809692>, arXiv:0903.0721.
- [29] Frinchaboy PM, Majewski SR. Open clusters as Galactic disk tracers. I. Project motivation, cluster membership, and bulk three-dimensional kinematics. *Astron J* 2008;136:118–45. <http://dx.doi.org/10.1088/0004-6256/136/1/118>, arXiv:0804.4630.
- [30] Durand S, Acker A, Zijlstra A. The kinematics of 867 Galactic planetary nebulae. *Astron Astrophys Suppl* 1998;132:13–20. <http://dx.doi.org/10.1051/aas:1998356>.
- [31] Pont F, Queloz D, Bratschi P, Mayor M. Rotation of the outer disc from classical cepheids. *Astron Astrophys* 1997;318:416–28. <http://adsabs.harvard.edu/abs/1997A%26A...318...416P>.
- [32] Demers S, Battinelli P. C stars as kinematic probes of the Milky Way disk from 9 to 15 kpc. *Astron Astrophys* 2007;473:143–8. <http://dx.doi.org/10.1051/0004-6361:20077691>.
- [33] Battinelli P, Demers S, Rossi C, Gigoyan KS. Extension of the C star rotation curve of the Milky Way to 24 kpc. *Astrophysics* 2013;56:68–75. <http://dx.doi.org/10.1007/s10511-013-9268-7>, arXiv:1212.1116.
- [34] Reid MJ, Menten KM, Brunthaler A, Zheng XW, Dame TM, Xu Y, et al. Trigonometric parallaxes of high mass star forming regions: the structure and kinematics of the Milky Way. *Astrophys J* 2014;783:130. <http://dx.doi.org/10.1088/0004-637X/783/2/130>, arXiv:1401.5377.
- [35] Honma M, Nagayama T, Ando K, Bushimata T, Choi YK, Handa T, et al. Fundamental parameters of the Milky Way galaxy based on VLBI astrometry. *Publ Astron Soc Japan* 2012;64:136. <http://dx.doi.org/10.1093/pasj/64.6.136>, arXiv:1211.3843.
- [36] Stepanishchev AS, Bobylev VV. Galactic rotation curve from the space velocities of selected masers. *Astron Lett* 2011;37:254–66. <http://dx.doi.org/10.1134/S1063773711030054>.
- [37] Xu Y, Li JJ, Reid MJ, Menten KM, Zheng XW, Brunthaler A, et al. On the nature of the local spiral arm of the Milky Way. *Astrophys J* 2013;769:15. <http://dx.doi.org/10.1088/0004-637X/769/1/15>, arXiv:1304.0526.
- [38] Bobylev VV, Bajkova AT. Galactic rotation curve and spiral density wave parameters from 73 masers. *Astron Lett* 2013;39:809–18. <http://dx.doi.org/10.1134/S1063773713120037>, arXiv:1310.7189.
- [39] Schönrich R, Binney J, Dehnen W. Local kinematics and the local standard of rest. *Mon Not R Astron Soc* 2010;403:1829–33. <http://dx.doi.org/10.1111/j.1365-2966.2010.16253.x>, arXiv:0912.3693.
- [40] Merrifield MR. The rotation curve of the Milky Way to  $2.5 R_0$  from the thickness of the H I layer. *Astron J* 1992;103:1552–63. <http://dx.doi.org/10.1086/116168>.
- [41] Gillessen S, Eisenhauer F, Trippe S, Alexander T, Genzel R, Martins F, et al. Monitoring stellar orbits around the massive black hole in the Galactic center. *Astrophys J* 2009;692:1075–109. <http://dx.doi.org/10.1088/0004-637X/692/2/1075>.
- [42] Ando K, Nagayama T, Omodaka T, Handa T, Imai H, Nakagawa A, et al. Astrometry of Galactic star-forming region ON2N with VERA: estimation of the Galactic constants. *Publ Astron Soc Japan* 2011;63:45. <http://dx.doi.org/10.1093/pasj/63.1.45>.
- [43] Malkin Z. 2012. The current best estimate of the Galactocentric distance of the Sun based on comparison of different statistical techniques. ArXiv e-prints, arXiv:1202.6128.
- [44] Reid MJ, Brunthaler A. The proper motion of sagittarius A\*. II. The mass of sagittarius A\*. *Astrophys J* 2004;616:872–84. <http://dx.doi.org/10.1086/424960>, arXiv:astro-ph/0408107.
- [45] Reid MJ, Menten KM, Zheng XW, Brunthaler A, Moscadedelli L, Xu Y, et al. Trigonometric parallaxes of massive star-forming regions. VI. Galactic structure, fundamental parameters, and noncircular motions. *Astrophys J* 2009;700:137–48. <http://dx.doi.org/10.1088/0004-637X/700/1/137>.
- [46] Bovy J, Hogg DW, Rix H-W. Galactic masers and the Milky Way circular velocity. *Astrophys J* 2009;704:1704–9. <http://dx.doi.org/10.1088/0004-637X/704/2/1704>.
- [47] McMillan PJ, Binney JJ. The uncertainty in Galactic parameters. *Mon Not R Astron Soc* 2010;402:934–40. <http://dx.doi.org/10.1111/j.1365-2966.2009.15932.x>.
- [48] Bovy J, Allende Prieto C, Beers TC, Bizyaev D, da Costa LN, Cunha K, et al. The Milky Way's circular-velocity curve between 4 and 14 kpc from APOGEE data. *Astrophys J* 2012;759:131. <http://dx.doi.org/10.1088/0004-637X/759/2/131>.
- [49] Dehnen W, Binney JJ. Local stellar kinematics from HIPPARCOS data. *Mon Not R Astron Soc* 1998;298:387–94. <http://dx.doi.org/10.1046/j.1365-8711.1998.01600.x>.
- [50] [Astropy Collaboration], Robitaille TP, Tollerud EJ, Greenfield P, Droettboom M, Bray E, Aldcroft T, et al. Astropy: A community Python package for astronomy. *Astron Astrophys* 2013;558:A33. <http://dx.doi.org/10.1051/0004-6361/201322068>, arXiv:1307.6212.
- [51] Pato M, Iocco F, Bertone G. Dynamical constraints on the dark matter distribution in the Milky Way. *J Cosmology Astropart Phys* 2015;12:1. <http://dx.doi.org/10.1088/1475-7516/2015/12/001>, arXiv:1504.06324.
- [52] Pato M, Iocco F. The dark matter profile of the Milky Way: a non-parametric reconstruction. *Astrophys J* 2015;803:L3. <http://dx.doi.org/10.1088/2041-8205/803/1/L3>, arXiv:1504.03317.
- [53] Iocco F, Pato M, Bertone G. Testing modified Newtonian dynamics in the Milky Way. *Phys Rev* 2015;D92:084046. <http://dx.doi.org/10.1103/PhysRevD.92.084046>, arXiv:1505.05181.
- [54] Calore F, Bozorgnia N, Lovell M, Bertone G, Schaller M, Frenk CS, et al. Simulated Milky Way analogues: implications for dark matter indirect searches. *J Cosmology Astropart Phys* 2015;1512(12):053. <http://dx.doi.org/10.1088/1475-7516/2015/12/053>, arXiv:1509.02164.
- [55] Bozorgnia N, Calore F, Schaller M, Lovell M, Bertone G, Frenk CS, et al. Simulated Milky Way analogues: implications for dark matter direct searches. *J Cosmology Astropart Phys* 2016;1605(05):024. <http://dx.doi.org/10.1088/1475-7516/2016/05/024>, arXiv:1601.04707.
- [56] Sofue Y. Rotation curve and mass distribution in the Galactic center – from black hole to entire galaxy. *Publ Astron Soc Jap* 2013;65:118. <http://dx.doi.org/10.1093/pasj/65.6.118>, arXiv:1307.8241.
- [57] Chemin L, Renaud F, Soubiran C. Incorrect rotation curve of the Milky Way. *Astron Astrophys* 2015;578:A14. <http://dx.doi.org/10.1051/0004-6361/201526040>, arXiv:1504.01507.
- [58] Dehnen W, McLaughlin DE, Sachania J. The velocity dispersion and mass profile of the Milky Way. *Mon Not R Astron Soc* 2006;369:1688–92. <http://dx.doi.org/10.1111/j.1365-2966.2006.10404.x>, arXiv:astro-ph/0603825.
- [59] Xue XX, Rix HW, Zhao G, Re Fiorentin P, Naab T, Steinmetz M, et al. The Milky Way's circular velocity curve to 60 kpc and an estimate of the dark matter halo mass from the kinematics of  $\sim 2400$  SDSS blue horizontal-branch stars. *Astrophys J* 2008;684:1143–58. <http://dx.doi.org/10.1086/589500>, arXiv:0801.1232.
- [60] Kafle PR, Sharma S, Lewis GF, Bland-Hawthorn J. Kinematics of the stellar halo and the mass distribution of the Milky Way using blue horizontal branch stars. *Astrophys J* 2012;761:98. <http://dx.doi.org/10.1088/0004-637X/761/2/98>, arXiv:1210.7527.
- [61] Kafle PR, Sharma S, Lewis GF, Bland-Hawthorn J. On the shoulders of giants: properties of the stellar halo and the Milky Way mass distribution. *Astrophys J* 2014;794:59. <http://dx.doi.org/10.1088/0004-637X/794/1/59>, arXiv:1408.1787.
- [62] Bovy J, Rix H-W. A direct dynamical measurement of the Milky Way's disk surface density profile, disk scale length, and dark matter profile at 4 kpc  $< R < 9$  kpc. *Astrophys J* 2013;779:115. <http://dx.doi.org/10.1088/0004-637X/779/2/115>, arXiv:1309.0809.

- [63] Loebman SR, Ivezić Ž, Quinn TR, Bovy J, Christensen CR, Jurić M, et al. The Milky Way tomography with sloan digital sky survey. V. Mapping the dark matter halo. *Astrophys J* 2014;794:151. <http://dx.doi.org/10.1088/0004-637X/794/2/151>, arXiv:1408.5388.
- [64] Russeil D. Star-forming complexes and the spiral structure of our galaxy. *Astron Astrophys* 2003;397:133–46. <http://dx.doi.org/10.1051/0004-6361/20021504>.
- [65] Kuijken K, Gilmore G. The Galactic disk surface mass density and the Galactic force  $K(z)$  at  $Z = 1.1$  kiloparsecs. *Astrophys J* 1991;367:L9–13. <http://dx.doi.org/10.1086/185920>.
- [66] Holmberg J, Flynn C. The local surface density of disc matter mapped by Hipparcos. *Mon Not R Astron Soc* 2004;352:440–6. <http://dx.doi.org/10.1111/j.1365-2966.2004.07931.x>, arXiv:astro-ph/0405155.
- [67] Moni Bidin C, Carraro G, Méndez RA, Smith R. Kinematical and chemical vertical structure of the Galactic thick disk. II. A lack of dark matter in the solar neighborhood. *Astrophys J* 2012;751:30. <http://dx.doi.org/10.1088/0004-637X/751/1/30>, arXiv:1204.3924.
- [68] Bovy J, Tremaine S. On the local dark matter density. *Astrophys J* 2012;756:89. <http://dx.doi.org/10.1088/0004-637X/756/1/89>, arXiv:1205.4033.
- [69] Moni Bidin C, Smith R, Carraro G, Méndez RA, Moyano M. On the local dark matter density. *Astron Astrophys* 2015;573:A91. <http://dx.doi.org/10.1051/0004-6361/201424675>, arXiv:1411.2625.
- [70] Garbari S, Read JI, Lake G. Limits on the local dark matter density. *Mon Not R Astron Soc* 2011;416:2318–40. <http://dx.doi.org/10.1111/j.1365-2966.2011.19206.x>, arXiv:1105.6339.
- [71] Smith MC, Whiteoak SH, Evans NW. Slicing and dicing the Milky Way disk in the sloan digital sky survey. *Astrophys J* 2012;746:181. <http://dx.doi.org/10.1088/0004-637X/746/2/181>, arXiv:1111.6920.
- [72] Garbari S, Liu C, Read JI, Lake G. A new determination of the local dark matter density from the kinematics of K dwarfs. *Mon Not R Astron Soc* 2012;425:1445–58. <http://dx.doi.org/10.1111/j.1365-2966.2012.21608.x>, arXiv:1206.0015.
- [73] Zhang L, Rix H-W, van de Ven G, Bovy J, Liu C, Zhao G. The gravitational potential near the sun from SEGUE K-dwarf kinematics. *Astrophys J* 2013;772:108. <http://dx.doi.org/10.1088/0004-637X/772/2/108>, arXiv:1209.0256.
- [74] Read JI. The local dark matter density. *J Phys G. Nucl. Phys* 2014;41(6):063101. <http://dx.doi.org/10.1088/0954-3899/41/6/063101>, arXiv:1404.1938.
- [75] Sofue Y, Honma M, Omodaka T. Unified rotation curve of the galaxy – decomposition into de Vaucouleurs bulge, disk, dark halo, and the 9-kpc rotation dip. *Publ Astron Soc Japan* 2009;61:227. <http://dx.doi.org/10.1093/pasj/61.2.227>, arXiv:0811.0859.
- [76] Catena R, Ullio P. A novel determination of the local dark matter density. *J Cosmol Astropart Phys* 2010;8:4. <http://dx.doi.org/10.1088/1475-7516/2010/08/004>, arXiv:0907.0018.
- [77] Weber M, de Boer W. Determination of the local dark matter density in our galaxy. *Astron Astrophys* 2010;509:A25. <http://dx.doi.org/10.1051/0004-6361/200913381>, arXiv:0910.4272.
- [78] Salucci P, Nesti F, Gentile G, Frigerio Martins C. The dark matter density at the Sun's location. *Astron Astrophys* 2010;523:A83. <http://dx.doi.org/10.1051/0004-6361/201014385>, arXiv:1003.3101.
- [79] Iocco F, Pato M, Bertone G, Jetzer P. Dark matter distribution in the Milky Way: microlensing and dynamical constraints. *J Cosmol Astropart Phys* 2011;11:29. <http://dx.doi.org/10.1088/1475-7516/2011/11/029>, arXiv:1107.5810.
- [80] McMillan PJ. Mass models of the Milky Way. *Mon Not R Astron Soc* 2011;414:2446–57. <http://dx.doi.org/10.1111/j.1365-2966.2011.18564.x>, arXiv:1102.4340.
- [81] Nesti F, Salucci P. The dark matter halo of the Milky Way, AD 2013. *J Cosmol Astropart Phys* 2013;7:16. <http://dx.doi.org/10.1088/1475-7516/2013/07/016>, arXiv:1304.5127.
- [82] Nesti F, Salucci P. The dark matter halo of the Milky Way, AD 2013. *J Cosmol Astropart Phys* 2013;1307:016. <http://dx.doi.org/10.1088/1475-7516/2013/07/016>, arXiv:1304.5127.
- [83] Sofue Y. 2015, Dark halos of M31 and the Milky Way, ArXiv e-prints, arXiv:1504.05368.
- [84] Bania TM. Carbon monoxide in the inner galaxy. *Astrophys J* 1977;216:381–403. <http://dx.doi.org/10.1086/155478>.
- [85] Liszt HS, Burton WB, Sanders RH, Scoville NZ. Kinematics of carbon monoxide observed within one degree of the Galactic center. *Astrophys J* 1977;213:38–42. <http://dx.doi.org/10.1086/155125>.
- [86] Alvarez H, May J, Bronfman L. The rotation of the Galaxy within the solar circle. *Astrophys J* 1990;348:495–502. <http://dx.doi.org/10.1086/168258>.
- [87] Dias WS, Alessi BS, Moitinho A, Lépine JRD. New catalogue of optically visible open clusters and candidates. *Astron Astrophys* 2002;389:871–3. <http://dx.doi.org/10.1051/0004-6361:20020668>, arXiv:astro-ph/0203351.
- [88] Zhang CY. A statistical distance scale for Galactic planetary nebulae. *Astrophys J Suppl* 1995;98:659–78. <http://dx.doi.org/10.1086/192173>.
- [89] Zhang CY. On the distance to Galactic planetary nebulae. *Astrophys J* 1993;410:239–50. <http://dx.doi.org/10.1086/172740>.